Title

Climate change impacts plant carbon balance, increasing mean future carbon use efficiency but decreasing total forest extent at dry range edges

Permalink

https://escholarship.org/uc/item/6kx199dx

Author

Trugman, Anna

Publication Date

2021

Peer reviewed

LETTER

ECOLOGY LETTERS   cnrs   WILEY

Climate change impacts plant carbon balance, increasing mean future carbon use efficiency but decreasing total forest extent at dry range edges

Justin M. Mathias (ORCID) | **Anna T. Trugman** (ORCID)

Department of Geography, University of California, Santa Barbara, Santa Barbara, California, USA

Correspondence
Justin M. Mathias, Department of Geography, University of California, Santa Barbara, 1832 Ellison, Santa Barbara, CA, USA.
Email: justin.m.mathias@gmail.com

Abstract

Carbon use efficiency (CUE) represents how efficient a plant is at translating carbon gains through gross primary productivity (GPP) into net primary productivity (NPP) after respiratory costs (R_a). CUE varies across space with climate and species composition, but how CUE will respond to climate change is largely unknown due to uncertainty in R_a at novel high temperatures. We use a plant physiological model validated against global CUE observations and LIDAR vegetation canopy height data and find that model-predicted decreases in CUE are diagnostic of transitions from forests to shrubland at dry range edges. Under future climate scenarios, we show mean growing season CUE increases in core forested areas, but forest extent decreases at dry range edges, with substantial uncertainty in absolute CUE due to uncertainty in R_a. Our results highlight that future forest resilience is nuanced and controlled by multiple competing mechanisms.

KEYWORDS
carbon use efficiency, climate change, forest range limits, temperature dependence of respiration, vegetation model

INTRODUCTION

Forests are one of the largest conduits in the transfer of carbon from Earth's atmosphere to the terrestrial biosphere, providing a sink for *ca.* 2.4 Pg C annually and accounting for nearly half of terrestrial net primary productivity (NPP) (Field, 1998; Pan et al., 2011). However, NPP represents only a fraction of the total amount of carbon fixed during photosynthesis (GPP), as a substantial amount of CO_2 is released back to the atmosphere through autotrophic respiration (R_a) (Field, 1998). Indeed, observations from trees around the world show between *ca.* 20 and 80% of GPP may be partitioned to R_a (Collalti & Prentice, 2019; DeLucia et al., 2007). This translates to a similarly large range in tree carbon use efficiency (CUE), or the ratio of tree NPP to GPP, which is an integrated index that tracks and allows direct comparison of tree carbon metabolism across a range of productivity (DeLucia et al., 2007).

Some of the spatial patterns in tree CUE can be explained by tree age (DeLucia et al., 2007; Mäkelä & Valentine, 2001), disturbance history (Kunert et al., 2019), species richness (Kunert et al., 2019) and tree functional type (Chen & Yu, 2019; Collalti & Prentice, 2019). Tree CUE also varies appreciably across climate-space, tending to decrease with increasing temperature in juvenile (Drake et al., 2019) and mature trees (Chen & Yu, 2019; He et al., 2018). Yet, how tree CUE may change as a result of increasing atmospheric CO_2 (eCO_2) has been given less attention. On one hand, eCO_2 stimulates leaf-level photosynthesis (i.e. GPP) (Ainsworth & Rogers, 2007) and has driven increases in tree leaf area (Zhu et al., 2016), which may be reflected in higher NPP (Mathias & Thomas, 2018; Norby et al., 2005; Walker et al., 2019), and result in increasing tree CUE, especially if NPP is stimulated proportionally more than GPP. Alternatively, if eCO_2-driven increases in leaf area, which requires similar additional investment in roots for water uptake and

transport (Litton et al., 2007; Nie et al., 2013), result in proportionately higher costs (R_a) than benefits (NPP or GPP), tree CUE may decline.

The future trajectory of tree CUE may be even more uncertain when considering the combined effects of eCO$_2$ and climate change on NPP, GPP and R_a. While the short- and long-term responses of leaf-level photosynthesis to eCO$_2$ and environment are relatively well documented (Ainsworth & Rogers, 2007; Bernacchi et al., 2001, 2013; Farquhar et al., 1980; Farquhar & Sharkey, 1982) and have been incorporated widely into process-based models, future changes in R_a may contribute a large source of uncertainty, and therefore a potential source of variability in estimates of future forest CUE and the terrestrial carbon cycle. Some uncertainty is related to the nature and extent of acclimation of R_a over longer time periods (Atkin & Tjoelker, 2003; Lombardozzi et al., 2015; Slot et al., 2014; Smith et al., 2016). However, the explicit representation of the temperature–respiration relationship is also critical to consider (Heskel et al., 2016; Reich et al., 2016). A wide range of functions grounded on robust empirical relationships has been developed to represent how R_a varies across a range of temperatures (Arrhenius, 1889; Gillooly, 2001; Heskel et al., 2016; Lloyd & Taylor, 1994), with each predicting similar R_a at moderate temperatures. However, across the suite of temperature–respiration functions, predictions of R_a diverge at novel high temperatures that are anticipated in some regions of the globe with warming under future climate change, with potential CUE and carbon cycle consequences that are important to understand.

Here, we leverage a physiologically based tree model that couples carbon allocation to local environmental conditions through gas exchange and plant hydraulic transport (Trugman, Detto, et al., 2018) to examine the consequences of eCO$_2$ and climate change on future tree CUE globally. We first update the model to incorporate the temperature dependency of C$_3$ photosynthesis and tissue respiration. We then ask 1) how does the model-predicted CUE across six different respiration functions commonly utilised in Earth system models compare with observations of CUE from trees around the world across a range of climates, 2) what are the consequences of eCO$_2$ and future projections of climate change on tree CUE globally and 3) what do changes in the distribution of CUE globally tell us about the future of forests in a changing climate?

MATERIALS AND METHODS

Model overview

The physiologically based tree model, adapted from Trugman, Detto, et al. (2018), couples carbon allocation to local environmental conditions through gas exchange and plant hydraulic transport. The original model (see Trugman, Detto, et al., 2018 for full model description) requires inputs of atmospheric CO$_2$ (C$_a$, ppm), vapour pressure deficit (VPD, Pa) and soil water potential (Ψ_{soil}, MPa). Here, we update the model to include a tree physiological response of photosynthesis and respiration to temperature (T_{air}, °C), such that in the updated model inputs include C$_a$, VPD, Ψ_{soil} and T_{air}, as described below. The rate of carbon fixation during photosynthesis is assumed to be limited by Rubisco (Trugman, Detto, et al., 2018) with a full description in the supporting information.

The temperature dependence of respiration has been documented empirically using a range of functions, all of which result in similar predictions for R_a at temperatures below 36.5°C. However, estimates of R_a diverge at temperatures above 36.5°C. The divergence of data-constrained respiration functions at higher temperatures has significant consequences for our understanding of carbon partitioning under novel expected high temperatures and therefore tree CUE under climate change. Thus, we calculated the sensitivity of leaf (light and dark), stem (xylem and phloem) and root respiration using each of six temperature–respiration response functions (Figure S1) which represent a spectrum of decreasing sensitivity to temperature, in turn: 1) Arrhenius, 2) fixed Q$_{10}$, 3) universal temperature dependence, 4) log-polynomial, 5) Lloyd-Taylor or a 6) variable Q$_{10}$ function in the absence of short- or long-term thermal acclimation (see Supporting Information Methods for the full equations). When simulating the sensitivity of CUE to respiration functional form, the same respiration function was used across all biomass pools.

Across all respiration functions, leaf respiration in light ($R_{leaflight}$) was calculated as a temperature-dependent variable fraction (0.66–0.80) of leaf respiration in dark ($R_{leafdark}$) following Way et al. (2015) using

$$R_{leaflight} = R_{leafdark} \times (0.0039 \times T + 0.6219). \quad (1)$$

A tree stem respiration at 25°C of 0.719 µmol CO$_2$ m^{-2} s^{-1} was used (Edwards & Hanson, 1996) and partitioned into the xylem (~21% of total stem respiration) and phloem respiration (~79% of total) following Stockfors and Linder (1998). Whole-tree NPP is calculated as GPP minus R_a, and tree CUE as the ratio of NPP to GPP.

Model validation

We validated model performance in two ways. First, we directly compared model-simulated CUE with a compilation of site-level estimates of forest CUE ($N = 228$) (Collalti & Prentice, 2019) across a range of mean growing season temperatures (10–28°C). We ran separate model simulations for each of the six respiration functions, in turn. Second, we examined model skill in capturing vegetation transitions at dry range edges by

performing a series of global simulations and examining spatial patterns of CUE.

For the first model validation (Figure S2, Table S2), we held all model parameters and inputs constant except T_{air}, which we varied from 10 to 45°C. Given that most measurements did not include detailed demographic or climate information, we used CO_2, DBH, Ψ_{soil}, and VPD values of 415 ppm, 30 cm, −0.3 MPa and 800 Pa, respectively. Tree *leaf area* (m^2) was calculated to maximise whole tree NPP (Trugman et al., 2019) while varying T_{air} across 10–45°C and keeping other climate factors fixed using the *optimise()* function from the 'stats' package in R (R Core Team, 2018). We limited the maximum *leaf area* to 1600 m^2, assuming the relationship between tree DBH and leaf area described in Forrester et al. (2017) for broadleaf and needle leaf trees is widely conserved (Figure S3). We then compared model-predicted CUE with the distribution of published tree CUE observations across temperatures (Collalti & Prentice, 2019). Given that growing season T_{air} was not included with the CUE observations (Collalti & Prentice, 2019), we extracted growing season T_{air} for the time period 1980–2009 for each study location (based on documented site GPS coordinates) with a unique CUE observation using the Climatic Research Unit (CRU TS4.03) global-gridded data product (Harris & Jones, 2019), which we then used to calculate 30-year growing season mean T_{air}, assuming that photosynthesis primarily occurs during June, July and August for the northern hemisphere (≥0° latitude) and December, January and February for the southern hemisphere (≤0° latitude). To determine where model-prognosed CUE significantly diverged among the functions examined, we performed a breakpoint analysis of the range in model-predicted CUE (i.e. CUE_{max} – CUE_{min}) as a function of temperature across the six respiration functions using the R package 'segmented' (Muggeo, 2008). Linear regression was used to determine the relationship between temperature and modelled tree CUE prior to the estimated breakpoint.

For the second model validation, we ran global simulations with one modelled tree per grid cell and examined the spatial patterns in CUE (Figure S3). We compared spatial patterns in model-predicted CUE to a LIDAR-based canopy height data set that documents transitions from forests to shrubland to examine whether the model was a useful tool for predicting where trees could exist at dry range edges. Specifically, for our global model simulations, we initialised each pixel with a tree 14 m in height (though we found CUE to be invariant to tree size, Table S3) and calculated tree DBH (13.5 cm) from height following Farrior et al. (2013). Functional tree xylem cross-sectional area (A_x, m^2) was estimated from DBH as *ca.* 62% of total xylem cross-sectional area (Trugman, Detto, et al., 2018). Environmental forcings for the model including mean temperature (T_{air}, °C; calculated as the average of T_{max} and T_{min}) and VPD were extracted from TerraClimate (Abatzoglou et al., 2018). Soil moisture (SM, kg H_2O m^{-2}

soil) was extracted from the NASA Global Land Data Assimilation System Version 2 (GLDAS-2) (Beaudoing & Rodell, 2020; Rodell et al., 2004) for 2005, the same year during which LIDAR canopy height retrievals were made. We converted SM to soil volumetric water content (θ, m^3 H_2O m^{-3} soil), integrating over the soil depth profile for each soil layer down to 2 m, which we weighted by the biome-specific distribution of roots throughout the soil horizon (Schenk & Jackson, 2002) within each respective biome in which trees grow, excluding mangroves (Dinerstein et al., 2017). We then calculated soil water potential (Ψ_{soil}, MPa) from θ using

$$\Psi_s = \Psi_{sat} \times \left(\frac{\theta}{\theta_{sat}} \right)^{-b}, \qquad (2)$$

where Ψ_{sat} is the saturated soil water potential (MPa), θ_{sat} is the saturated volumetric water content of the soil (m^3 H_2O m^{-3} soil), and b is the Clapp-Hornberger coefficient (unitless) (Clapp & Hornberger, 1978), which are specific to a given soil type and were determined using data products from the Global Soil Wetness Project – Phase 2 (Dirmeyer et al., 2002). In cases, where Ψ_{soil} became highly negative (i.e. <−10 MPa), a value of −10 MPa was assigned. We calculated growing season means for each environmental factor for each respective period as described previously. All global gridded data products were resampled to the same extent (0.1° × 0.1°) using the *resample()* function in the 'raster' package in R using a bilinear method (Hijmans, 2020) for analyses. We optimised leaf area for each tree within each grid cell, given grid-specific environmental forcings to calculate the tree CUE.

We compared simulated tree CUE against a high-resolution (1 × 1 km) LIDAR vegetation canopy height data product from the Geoscience Laser Altimeter System (GLAS) on the Ice, Cloud, and land Elevation Satellite (ICESat) retrieved during 2005 (Simard et al., 2011). Vegetation with canopy height <2 m was excluded from analyses following the International Geosphere-Biosphere Land classification system (Loveland & Belward, 1997). This analysis allowed us to examine the relationship between forest canopy height and model-predicted CUE for each grid cell using a two-dimensional density kernel estimation, breakpoint analysis, and linear regression.

Model experiments: Historical and future climate forcing data

To understand the sensitivity of forest CUE to potential changes in climate associated with anthropogenic climate change, we used globally gridded data products from a representative subset of 7 coupled climate-Earth System Models (ESMs) from the Coupled Model Intercomparison Project-Phase 5 (CMIP5) for the periods 1976–2005 (historical) and 2071–2100 (future Respective Concentration Pathway 8.5, *hereafter* RCP8.5) for our

analyses (see, Figure S5, Table S4) (Taylor et al., 2012). We accessed the Centre for Environmental Data Access data portal (https://www.ceda.ac.uk) to download monthly averages for each climate variable, mean air temperature (T_{air}, °C), surface air pressure (P_s, Pa), soil moisture (SM, kg H_2O m^{-2} soil), and relative humidity (RH, %) for each respective period of interest. We calculated vapour pressure deficit (VPD, Pa) from RH, T_{air}, and P_s using the function *RHtoVPD()* in the 'plantecophys' R package (Duursma, 2015) and Ψ_{soil} from soil moisture as described previously. Similar to our model validation simulations, we calculated growing season mean climatologies over the 30-year period for all environmental factors. We then computed the multi-model median value for each environmental factor for each grid cell when forcing the physiologically based tree model under historical and future scenarios. All global gridded data products were resampled to the same extent (0.1° × 0.1°) and were masked using the vegetation canopy height LIDAR product. Concentrations of atmospheric CO_2 used in our analysis for the historical and future periods were 354 ppm and 807 ppm (Meinshausen et al., 2011), respectively. We used two-dimensional kernel density estimation using the function *kde2d()* from the R package 'MASS' (Venables & Ripley, 2002), and linear regression, to quantify the relationship between temperature and tree height with modelled CUE at the global scale.

Model experiments: CUE under future climate

We examined the sensitivity of model-predicted CUE to two distinct climatological periods of 30 years: historical (1976–2005) and end-of-century (2071–2100, RCP8.5). Tree height was assigned according to LIDAR estimates (Simard et al., 2011). Tree leaf area was optimised based on grid cell-specific climate for each respective period (historical and future) using the CMIP5 growing season multi-model median value for each environmental factor (i.e. VPD, Ψ_{soil}, T_{air}) and the respective mean mid-year atmospheric CO_2 concentration (historical: 354 ppm, future: 807 ppm). We assumed no change in tree characteristics beyond leaf area between the historical and future simulations. We performed a series of model experiments designed to understand the sensitivity of tree CUE and forest extent to eCO_2 and climate change by first simulating historical and then future tree CUE, using leaf area and environmental factors specific to each time period. Finally, we examined the relative contribution of each environmental factor, CO_2, VPD, Ψ_{soil} and T_{air}, in isolation to the change in CUE between historical and future periods (ΔCUE) through factorial model experiments where we varied the environmental factor of interest each in isolation between the historical and future periods. For our global model experiments, we performed a one-way ANOVA to determine the change in global CUE across all respiration functions between historical and future climate scenarios.

CUE and forest biogeography

Our two-dimensional kernel density estimation indicated that model-predicted decreases in CUE corresponded to decreases in observed vegetation canopy height associated with transitions from taller forests to shorter shrubland at dry edge range limits for forests. Thus, we used model-predicted CUE to diagnose geographic areas where future forest range shifts may occur due to changes in hydroclimate. We consider geographic areas where future environmental conditions are insufficient to support tree growth as diagnosed by model-predicted negative CUE (i.e. R_a >GPP), as well as those areas that may experience possible forest expansion where future CUE is positive and historical CUE is negative. For this analysis, we examine three potential cases leveraging results from our historical–future climate simulations: 1) no change in forest range (i.e. no change in sign of CUE), 2) forest range expansion (i.e. negative CUE$_{historical}$ to positive CUE$_{future}$) and 3) forest range decline (i.e. positive CUE$_{historical}$ to negative CUE$_{future}$). We then examine the nature of the relationship between environmental factors and model CUE-derived range shifts, including non-forested biomes such as grasslands and shrublands, where future forest encroachment could be possible.

Model limitations

In the current model formulation and model predictions, we neglected the effects of spatial variability in plant traits that mediate forest biogeographic patterns. Although we do not account for spatial variability in functional traits, we found that model adjustments in leaf area covary with key traits regulating plant water demand (Table S1), largely compensating for potential spatial variability in traits such as V_{cmax25}. We also do not explicitly represent tree age in our framework. However, model predictions for forest transitions at dry range limits are consistent with observed spatial patterns in vegetation canopy height. Thus, we contend that our simple model framework will help inform understanding of how climate change and CO_2 fertilisation will impact forest extent and inform the uncertainty in these projections associated with our understanding of R_a.

RESULTS

Model validation and the sensitivity of CUE to climate

Compared to a meta-analysis of observed CUE across a range of climates globally spanning mean growing season temperatures of 12–28°C, model-predicted CUE intersected median observed CUE for temperatures 15 and 21°C (Figure 1a). As the temperature increased,

model-predicted CUE fell well within the interquartile range of observed CUE, however, model predictions were biased low relative to the observed median CUE values at a given temperature by 0.033 ± 0.008 (Table S2). Further, across the observed temperature ranges, model performance did not differ appreciably across the six respiration functions.

Despite the fact that model performance was roughly independent of respiration function choice across the observed range of CUE, the choice of respiration matters for high-temperature conditions expected with anthropogenic climate change. Specifically, across all six respiration functions, model-predicted CUE decreased, on average, by 0.12 for each 10°C increase in temperature ($R^2 = 0.97$, $p < 0.001$) up to 36.5 ± 0.45°C (Figure 1a), which is ~4.5°C higher than current average highs (*ca.* 32°C) observed in the tropics. However, as temperature increased above 36.5°C, CUE significantly diverged across the six respiration functions considered (Figure S5). At high temperature, the choice of respiration function is of critical importance, as CUE is least sensitive to increasing temperature under a variable Q_{10} representation of respiration sensitivity to temperature (analogous to some acclimation of respiration to temperature) and is most sensitive under an Arrhenius representation of respiration sensitivity to temperature (Figure 1a). Notably, no current observations of CUE exist at the high-temperature limit (36.5°C), where we find the respiration functions significantly diverge (Figure 1a, Figure S6). Thus, it is not currently possible to evaluate the functional performance of these respiration functions when it matters most. As a result, there is significant uncertainty related to future plant CUE in locations such as central North America, central South America and central Eurasia, where climate change is projected to increase growing season temperature above 36.5°C under some emissions scenarios (Figure S7).

Plant CUE is sensitive not only to temperature, because of the impact of temperature on respiration and GPP, but also plant available water, which influences the balance of plant productivity relative to maintenance respiration. We therefore quantified the sensitivity of plant CUE through our model to changes in environmental factors that influence water use based on global climatologies. Interestingly, we found that model-predicted CUE varies with the environment globally and the spatial variation is driven by two climatic regions with distinct mechanisms at play—cool high latitude forest areas with a relatively high CUE due to low respiration and warm forested areas that transition from wet forests with intermediate CUE values to dry forests with low CUE (Figure 2a; Figure S8), and ultimately shrublands and grasslands (which our model is not designed to represent). The bimodal distribution of modelled CUE values ranged from *ca.* 0–0.70, with a median value of 0.42 across the six respiration representations (Figure 2), and the highest densities of model-predicted CUE occurred at growing season temperatures *ca.* 14.7 and *ca.* 26.5°C, corresponding to tree CUE of 0.48 and 0.35, respectively (Figure 2b, Figures S9, S10a). Compared to observations of canopy height across hydroclimate gradients, we found that transitions from taller forests at 13.4 ± 0.01 m to shorter shrubland corresponded with rapid decreases in model-prognosed CUE from ~0.5 to values that are unsustainable by trees over prolonged periods at a rate of ~0.021 CUE/m decrease in canopy height ($p < 0.001$) (Figure 2c; Figures S10b, S11), particularly at dry range limits of forests (Figure 2a). Thus, the model was able to reproduce dry range edges based on tree CUE.

Model experiments: Climate change impacts on CUE and forest dry range edge extent

At the global scale, model-predicted CUE increased, on average, by 6.2% (*ca.* 0.024 ± 0.002, mean ± SE) between the historical (1976–2005) and the future (2071–2100) time periods ($F = 21.7$, $p < 0.001$; Table 1), driven predominantly by large increases in CO_2 which stimulated GPP (Figure 3). Future increases in $\bar{T}_{air}$ and VPD (Table S4) strongly reduced the realised increases due to CO_2, while future changes in Ψ_{soil} did not have an appreciable impact on mean global CUE (Figure 3, Table S4). However, the choice of respiration function introduced uncertainty
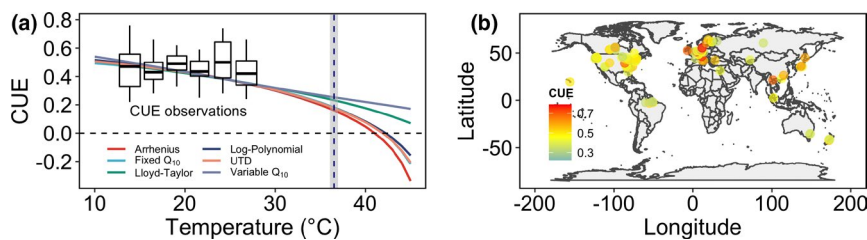
FIGURE 1 Model-predicted CUE across a range of temperature for six temperature-respiration functions (a) and locations of tree CUE observations (b). Solid colour lines in (a) represent model-predicted CUE using each of six temperature–respiration representations, while the boxplots in (a) correspond to published observations of CUE globally (Collalti & Prentice, 2019). Boxplots highlight the median, interquartile range and 95% CI for CUE observations across a range of temperatures. The colour of location markers in (b) represent the site-level estimate of CUE from Collalti and Prentice (2019) and correspond to the boxplots in panel (a). The horizontal dashed line in (a) is at 0, which represents the point at which model-predicted autotrophic respiration equals gross primary productivity. All respiration functions were solved to 25°C and exhibit larger differences as temperature increases above 36.5 ± 0.45°C, denoted by the vertical dark blue line and grey shading in (a)
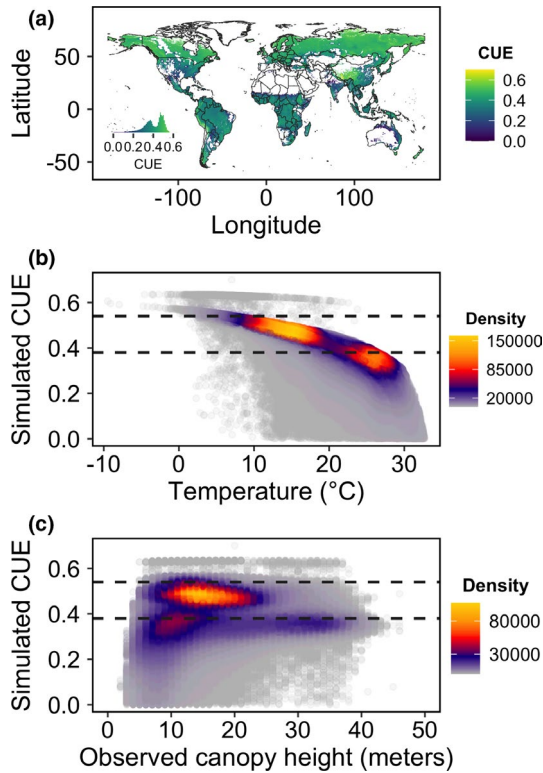
FIGURE 2 Carbon use efficiency (CUE) varies substantially globally (a), declines with increasing temperature (b) and explains dry edge forest range limits as forests transition to shrubland (c). Panel (a) shows model-predicted median CUE across six respiration functions for forested land areas (non-forest in white), with CUE values ranging from ~0 (dark purple) to 0.70 (yellow), with a global median of 0.42 across all forested pixels (0.1° × 0.1°). The inset in the lower left corner of (a) corresponds to the frequency distribution of tree CUE globally. Each individual data point in (b) and (c) corresponds to tree CUE in a 0.1° × 0.1° forested area predicted from the physiologically based tree model parameterised using global-gridded climate data (see Methods). The horizontal dashed lines in (b) and (c) correspond to the interquartile range (i.e. 25th and 75th percentile) of published observations of tree CUE ($N = 228$), while the colour of each data point represents the density of observations, with yellow being the highest density and grey being the lowest density

TABLE 1 Model-predicted global mean CUE values across seven CMIP5 models and six respiration functions examined in this study for two cases: 1) historical and 2) RCP8.5. The historical period spans the years 1976–2005, while the future period (RCP8.5) spans the years 2071–2100. ΔCUE represents the per cent change in CUE between the two periods

	Historical	RCP8.5	ΔCUE (%): RCP8.5–historical
Variable Q_{10}	0.432	0.452	+4.6
Lloyd-Taylor	0.418	0.448	+7.2
Log-Poly	0.425	0.447	+5.2
UTD	0.421	0.446	+5.9
Fixed Q_{10}	0.416	0.445	+7.0
Arrhenius	0.425	0.447	+5.2

into our predictions for both historical and future CUE, primarily due to the function-specific response of increasing T_{air} on respiration and therefore CUE (Table 1). Importantly, the variable Q_{10} respiration–temperature response function had the highest historical and future mean CUE values across all forested pixels (due to lower respiratory fluxes), while the fixed Q_{10} respiration representation showed the lowest global mean CUE within each respective period (Table 1), with a range in CUE across the six respiration functions (including historical and future CUE) of 0.036 or *ca.* 8.7%.

Given model skill in determining dry range limits in forest extent, we used model-predicted CUE to constrain where forest range shifts may occur under future climate scenarios. We found, on average across all respiration functions, a net reduction in *ca.* 105,124 km^2 of the forested area by 2100, driven by a decline of forested lands by 0.34% and an increase in forested lands by 0.19% (Table S5). Importantly, the balance between forest decline and increase is variable spatially, such that some biomes only experience forest range expansion or encroachment (i.e. flooded grasslands and tropical dry broadleaf) or no change (i.e. tundra), which is unsurprising because the model does not include mechanisms expected to govern forest cold edge limits, while the majority exhibit a variable range in the balance between forest range decline and increase (Figure 4, Table S6). Model-predicted CUE between historical and future periods shows boreal forests exhibit the largest net decline in forest range ($-61,895 \pm 528$ km^2) through the end of the 20th century, while land areas currently designated as flooded grasslands exhibit the largest potential for net forest area increase ($+373,939 \pm 74,545$ km^2) (Table S6). Furthermore, the choice of temperature–respiration representation mediated the sensitivity of our estimates of changes in future forested areas, with a variable Q_{10} representation resulting in larger increases and smaller declines in the net forested area and an Arrhenius representation resulting in larger declines and smaller increases in the net forested area (Figure 4, Table S6). As such, the differences in the temperature–respiration representation resulted in as little as a *ca.* 38,097 km^2 decline (variable Q_{10}) or as much as a *ca.* 150,313 km^2 decline (Arrhenius) in the net forested area globally in this analysis.

DISCUSSION

In this study, we use a physiologically based tree model to diagnose the underlying mechanisms and future uncertainties for forest resilience with anthropogenic-driven climate change. We capture observed dry range forest edges using a CUE framework where progressively lower model-predicted CUE corresponds with global vegetation height transitions from taller forested areas to shorter shrubland (Figure 2). We find that the future resilience of forests globally is nuanced, such that total
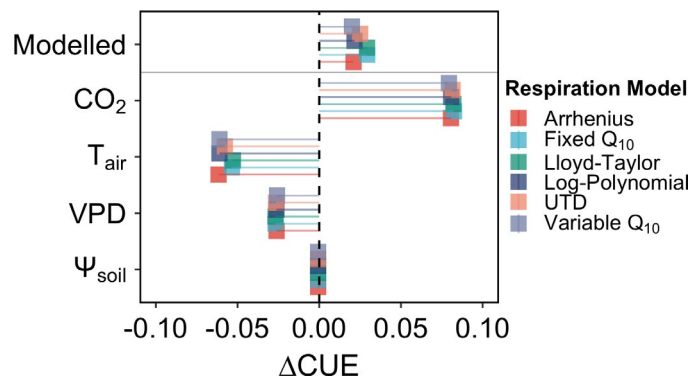
FIGURE 3 Model-predicted CUE increases globally by the end of the 21st century across each of the six temperature–respiration representations. Data points correspond to the absolute change in global mean CUE between the historical and the future period (i.e. CUE_{future} – $CUE_{historical}$) for each of the six temperature–respiration functions within a given model scenario. Model-predicted tree ΔCUE integrates the effects of each of the environmental factors CO_2, T_{air}, VPD and Ψ_{soil}, while each of the four additional scenarios represents a case of ΔCUE when only changing the respective factor of interest
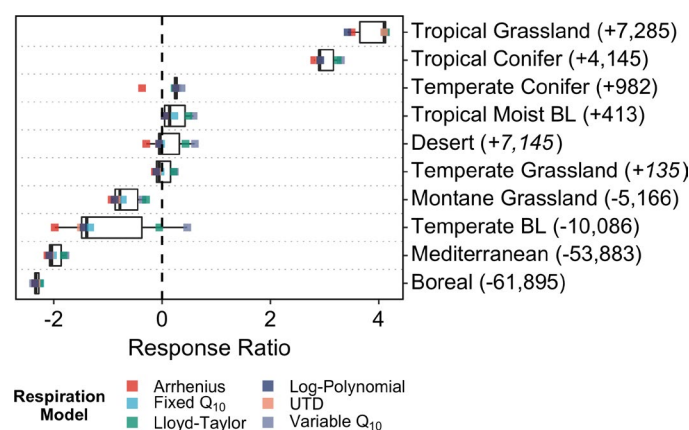
FIGURE 4 Model-simulated CUE informs potential changes in future forest ranges globally. The response ratio (RR) represents the natural log of increasing forested area divided by declining forested area within a given biome (i.e. RR = ln(area$_{increase}$/area$_{decline}$), such that more positive values represent much larger increases in the forested area or forest encroachment (in the case of grass or shrub biomes) relative to declines, while negative values indicate net declines in the forested area. Values in parentheses represent the net change in the forested area (km^2) for each biome. Italicised numbers indicate a case where the change in the forested area for a given biome was not significant. Not shown are flooded grasslands, tropical dry broadleaf forests and tundra, given they show only, in turn, increasing, increasing and no change in the forested area

forested area declines at dry range edges, but core forested areas exhibit overall higher mean CUE by the end of the 21st century (Figures 3, 4, Table 1). We show that uncertainty in our understanding of the sensitivity of R_a to increasing temperature introduces significant variability into predictions of CUE. Importantly, uncertainty is highest at higher temperatures that are expected with climate change but is currently unconstrained with observational data.

There currently exists no standardised representation of the temperature-R_a response in many widely used terrestrial biosphere models, with some adopting a fixed Q_{10} temperature–R_a function (e.g. Pnet-CN, ED2) (Medvigy et al., 2009; Thorn et al., 2015), others incorporating a variable Q_{10} function (e.g. CABLE) (Wang et al., 2007) and some scaling R_a with temperature and tissue nitrogen concentration (CLM4, JULES) (Clark et al., 2011; Oleson et al., 2013; Reich

et al., 2008). Our results highlight the consequences of the choice of temperature-R_a function by illustrating the large range in model-predicted CUE (driven primarily by R_a), which is too large to be ignored at high temperature (Figure S1). As autotrophic carbon fluxes, including R_a, increase towards warmer equatorial regions (Banbury Morgan et al., 2021), careful consideration of differences in modelled R_a becomes increasingly important for simulating future forest CUE, particularly when the temperature exceeds 36.5°C (Figure S7). Large-scale, data-rich experiments like SPRUCE (Hanson et al., 2017) will be invaluable in helping to constrain estimates of CUE at higher temperatures and CO_2.

Tree R_a is one of the largest, and also most challenging to measure, carbon fluxes globally. Yet, it is critical to accurately represent R_a in terrestrial biosphere models to understand climate change impacts

on forest resilience and the terrestrial carbon cycle. Multiple independent observations show that tree CUE declines with increasing temperature across the range of temperatures considered in this study (Chen & Yu, 2019; Dillaway & Kruger, 2014; He et al., 2018; Piao et al., 2010; Zhang et al., 2009), a phenomenon our physiologically based tree model reproduces. When considering the combined effects of multiple environmental factors globally, we find model-predicted tree CUE is higher in cool, moist ecosystems and lower in warm, dry ecosystems, trending to zero at forest dry range edges (Figure 2, Figure S8), similar to recent predictions using large-scale Earth-system models (which couple terrestrial biosphere models to the rest of the Earth system) and satellite retrievals (He et al., 2018). However, uncertainty remains. In an analysis by Collalti et al. (2020), the authors find that CUE increased with temperature in an observational range of up to ca. 28°C. Further, though the model and observations are in agreement with absolute CUE values in our analysis (Figure 1), a clear temperature trend is not evident in the observations. There are many reasons why these diverse measurements across space may not exhibit a clear temperature trend including diversity in species, diversity in tree ages, lack of site-specific soil moisture and VPD measurements at the time of observations and measurement uncertainty. Collectively, these results contextualise that our model results are in broad agreement with and additive to the literature but also highlight several future avenues of research (which we detail below).

Globally, variation in model-simulated tree CUE is driven by air temperature, VPD and soil water potential, reflecting our current knowledge of large-scale drivers of forest carbon cycling (Banbury Morgan et al., 2021; Fernández-Martínez et al., 2019; Humphrey et al., 2021). However, when considering end-of-century mean changes in simulated tree CUE, the effect of increasing atmospheric CO_2 stimulating GPP, on average, outweighs those environmental factors that either diminish GPP or stimulate R_a (Figure 4). The effects of increasing CO_2 and VPD on forest function have gained notable attention in recent years (Novick et al., 2016; Swann et al., 2016; Yuan et al., 2019), given their simultaneous, but often counteracting influences over tree physiology. In this context, our findings provide a unique framework to diagnose the areas where forests are vulnerable to climate driven die-off based on tree CUE (Figure 4). Indeed, the world's boreal forests, which are currently showing evidence of increasing browning and forest decline (Barber et al., 2000; Trugman, Medvigy, et al., 2018; Walker & Johnstone, 2014; Walker et al., 2015), experience the largest range decline of all biomes examined at dry range edges by the end of the 21st century as inferred through model-simulated CUE (Figure 4), and overwhelmingly contribute to the model-predicted global decline in forest range extent. The model-predicted declines in

temperate broadleaf forests are also consistent with reports from the southeastern United States (White et al., 2021). Moreover, these findings also agree with findings from a recent meta-analysis showing observations of widespread drought-induced tree mortality at dry range edges (Anderegg et al., 2019). However, despite model-predicted declines in the total forested area, projected increases in CO_2 resulted in higher mean CUE in areas that are predicted to maintain a positive CUE (Figure 3, Table 1). Targeted measurements of tree-level photosynthesis and respiration under experimental warming will be invaluable for assessing the extent to which these predictions are realised.

In conclusion, our analysis of tree CUE and forest dry range edges through the lens of a physiologically based tree model highlights the potential consequences and uncertainty of the choice of the temperature-R_a representation is widely used process-based models. Particularly, at higher temperatures, we show a variable Q_{10} representation, which represents some acclimation of respiration sensitivity to temperature, resulting in much less carbon being lost to R_a and consequently higher CUE. In contrast, an Arrhenius type representation yields the lowest tree CUE due to larger predicted R_a costs. Importantly, we find that model-predicted decreases in CUE correspond to decreases in observed vegetation canopy height associated with transitions from taller forests to shorter shrubland at dry range edges, indicating that model-predicted CUE is a useful tool for understanding future forest resilience to climate change-induced drought stress. Under future climate conditions, model predictions indicate an expected higher mean CUE in intact forest regions due to CO_2 fertilisation, but the declining geographic extent, highlighting that the resilience of forests under future climate change may be nuanced and controlled by multiple competing mechanisms.

AUTHORSHIP
JMM and ATT designed the study. ATT developed the original model which was updated by JMM in this study. JMM performed analyses and JMM and ATT wrote the final manuscript.

PEER REVIEW

OPEN RESEARCH BADGES

This article has earned an Open Materials badge for making publicly available the components of the research methodology needed to reproduce the reported procedure and analysis. All materials are available at: https://figshare.com/articles/software/tree_model/16645795. DOI: https://doi.org/10.6084/m9.figshare.16645795.vl.

DATA AVAILABILITY STATEMENT

All climate data used in this analysis are already publicly available. All analysis and model code are publicly available and archived at Figshare, https://doi.org/10.6084/m9.figshare.16645795.

ORCID

Justin M. Mathias https://orcid.org/0000-0001-5470-4167
Anna T. Trugman https://orcid.org/0000-0002-7903-9711

REFERENCES

Abatzoglou, J.T., Dobrowski, S.Z., Parks, S.A. & Hegewisch, K.C. (2018) TerraClimate, a high-resolution global dataset of monthly climate and climatic water balance from 1958–2015. *Scientific Data*, 5, 1–12.

Ainsworth, E.A. & Rogers, A. (2007) The response of photosynthesis and stomatal conductance to rising [CO_2]: mechanisms and environmental interactions. *Plant, Cell and Environment*, 30, 258–270.

Anderegg, W.R.L., Anderegg, L.D.L., Kerr, K.L. & Trugman, A.T. (2019) Widespread drought-induced tree mortality at dry range edges indicates that climate stress exceeds species' compensating mechanisms. *Global Change Biology*, 25, 3793–3802.

Arrhenius, S. (1889) Über die Reaktionsgeschwindigkeit bei der Inversion von Rohrzucker durch Säuren. Zeitschrift für Phys. Chemie, 4U.

Atkin, O. & Tjoelker, M.G. (2003) Thermal acclimation and the dynamic response of plant respiration to temperature. *Trends in Plant Science*, 8, 343–351.

Banbury Morgan, R., Herrmann, V., Kunert, N., Bond-Lamberty, B., Muller-Landau, H.C. & Anderson-Teixeira, K.J. (2021) Global patterns of forest autotrophic carbon fluxes. *Global Change Biology*, 15574, 2840–2855.

Barber, V.A., Juday, G.P. & Finney, B.P. (2000) Reduced growth of Alaskan white spruce in the twentieth century from temperature-induced drought stress. *Nature*, 405, 668–673.

Beaudoing, H., Rodell, M. & NASA/GSFC/HSL, (2020). GLDAS Noah Land Surface Model L4 monthly 0.25 x 0.25 degree V2.1. Available at: https://disc.gsfc.nasa.gov/datasets/GLDAS_NOAH025_M_2.1/summary?keywords=GLDAS Last accessed

Bernacchi, C.J., Bagley, J.E., Serbin, S.P., Ruiz-Vera, U.M., Rosenthal, D.M. & Vanloocke, A. (2013) Modelling C3 photosynthesis from the chloroplast to the ecosystem. *Plant, Cell and Environment*, 36, 1641–1657.

Bernacchi, C.J., Singsaas, E.L., Pimentel, C., Portis, A.R. Jr & Long, S.P. (2001) Improved temperature response functions for models of Rubisco-limited photosynthesis. *Plant, Cell and Environment*, 24, 253–259.

Chen, Z. & Yu, G. (2019) Spatial variations and controls of carbon use efficiency in China's terrestrial ecosystems. *Scientific Reports*, 9, 19516.

Clapp, R.B. & Hornberger, G.M. (1978) Empirical equations for some soil hydraulic properties. *Water Resources Research*, 14, 601–604.

Clark, D.B., Mercado, L.M., Sitch, S., Jones, C.D., Gedney, N., Best, M.J. et al. (2011) The joint UK land environment simulator (JULES), model description – Part 2: carbon fluxes and vegetation dynamics. *Geoscientific Model Development*, 4, 701–722.

Collalti, A., Ibrom, A., Stockmarr, A., Cescatti, A., Alkama, R., Fernández-Martínez, M. et al. (2020) Forest production efficiency increases with growth temperature. *Nature Communications*, 11, 5322.

Collalti, A. & Prentice, I.C. (2019) Is NPP proportional to GPP? Waring's hypothesis twenty years on. *Tree Physiology*, 04, 1–11.

DeLucia, E.H., Drake, J.E., Thomas, R.B. & Gonzalez-Meler, M. (2007) Forest carbon use efficiency: is respiration a constant fraction of gross primary production? *Global Change Biology*, 13, 1157–1167.

Dillaway, D.N. & Kruger, E.L. (2014) Trends in seedling growth and carbon-use efficiency vary among broadleaf tree species along a latitudinal transect in eastern North America. *Global Change Biology*, 20, 908–922.

Dinerstein, E., Olson, D., Joshi, A., Vynne, C., Burgess, N.D., Wikramanayake, E. et al. (2017) An ecoregion-based approach to protecting half the terrestrial realm. *BioScience*, 67, 534–545.

Dirmeyer, P.A., Gao, X. & Oki, T. (2002) *The Second Global Soil Wetness Project GSWP-2: Science and Implementation Plan*, Vol. 37. Washington, DC: U.S. Government Printing Office, pp. 1–75.

Drake, J.E., Tjoelker, M.G., Aspinwall, M.J., Reich, P.B., Pfautsch, S. & Barton, C.V.M. (2019) The partitioning of gross primary production for young Eucalyptus tereticornis trees under experimental warming and altered water availability. *New Phytologist*, 222, 1298–1312.

Duursma, R.A. (2015) Plantecophys—an R package for analysing and modelling leaf gas exchange data. *PLoS One*, 10, 1–13.

Edwards, N.T. & Hanson, P.J. (1996) Stem respiration in a closed-canopy upland oak forest. *Tree Physiology*, 16, 433–439.

Farquhar, G.D., Caemmerer, S.V., Berry, J.A. (1980) A biochemical model of photosynthesis CO_2 fixation in leaves of C3 species. *Planta*, 149, 78–90.

Farquhar, G.D. & Sharkey, T.D. (1982) Stomatal conductance and photosynthesis. *Annual Review of Plant Physiology*, 33, 317–345.

Farrior, C.E., Dybzinski, R., Levin, S.A. & Pacala, S.W. (2013) Competition for water and light in closed-canopy forests: a tractable model of carbon allocation with implications for carbon sinks. *American Naturalist*, 181, 314–330.

Fernández-Martínez, M., Sardans, J., Chevallier, F., Ciais, P., Obersteiner, M., Vicca, S. et al. (2019) Global trends in carbon sinks and their relationships with CO_2 and temperature. *Nature Climate Change*, 9, 73–79.

Field, C.B., Behrenfeld, M.J., Randerson, J.T. & Falkowski, P. (1998) Primary Production of the biosphere: integrating terrestrial and oceanic components. *Science (80-)*, 281, 237–240.

Forrester, D.I., Tachauer, I., Annighoefer, P., Barbeito, I., Pretzsch, H., Ruiz-Peinado, R. et al. (2017) Generalized biomass and leaf area allometric equations for European tree species incorporating stand structure, tree age and climate. *Forest Ecology and Management*, 396, 160–175.

Gillooly, J.F., Brown, J.H., West, G.B., Savage, V.M. & Charnov, E.L. (2001) Effects of size and temperature on metabolic rate. *Science (80-)*, 293, 2248–2251.

Hanson, P.J., Riggs, J.S., Nettles, W.R., Phillips, J.R., Krassovski, M.B., Hook, L.A. et al. (2017) Attaining whole-ecosystem warming using air and deep-soil heating methods with an elevated CO_2 atmosphere. *Biogeosciences*, 14, 861–883.

Harris, I.C. & Jones, P.D. (2019). CRU TS4.03: climatic Research Unit (CRU) Time-Series (TS) version 4.03 of high resolution gridded data of month-by-month variation in climate (Jan. 1901-Dec. 2018). Centre for Environmental Data Analysis.

He, Y., Piao, S., Li, X., Chen, A. & Qin, D. (2018) Global patterns of vegetation carbon use efficiency and their climate drivers deduced from MODIS satellite data and process-based models. *Agricultural & Forest Meteorology*, 256–257, 150–158.

Heskel, M.A., O'Sullivan, O.S., Reich, P.B., Tjoelker, M.G., Weerasinghe, L.K., Penillard, A. et al. (2016) Convergence in the temperature response of leaf respiration across biomes and plant functional types. *Proceedings of the National Academy of Sciences*, 113, 3832–3837.

Hijmans, R.J. (2020) raster: Geographic Data Analysis and Modeling. R package version 3.1-5.

Humphrey, V., Berg, A., Ciais, P., Gentine, P., Jung, M., Reichstein, M. et al. (2021) Soil moisture – atmosphere feedback dominates land carbon uptake variability. *Nature*, 592, 65–69.

Kunert, N., El-Madany, T.S., Aparecido, L.M.T., Wolf, S. & Potvin, C. (2019) Understanding the controls over forest carbon use efficiency on small spatial scales: effects of forest disturbance and tree diversity. *Agricultural & Forest Meteorology*, 269–270, 136–144.

Litton, C.M., Raich, J.W. & Ryan, M.G. (2007) Carbon allocation in forest ecosystems. *Global Change Biology*, 13, 2089–2109.

Lloyd, J. & Taylor, J.A. (1994) On the temperature dependence of soil respiration. *Functional Ecology*, 8, 315.

Lombardozzi, D.L., Bonan, G.B., Smith, N.G., Dukes, J.S. & Fisher, R.A. (2015) Temperature acclimation of photosynthesis and respiration: a key uncertainty in the carbon cycle-climate feedback. *Geophysical Research Letters*, 42, 8624–8631.

Loveland, T.R. & Belward, A.S. (1997) The international geosphere biosphere programme data and information System global land cover data set (DISCover). *Acta Astronautica*, 41, 681–689.

Mäkelä, A. & Valentine, H.T. (2001) The ratio of NPP to GPP: evidence of change over the course of stand development. *Tree Physiology*, 21, 1015–1030.

Mathias, J.M. & Thomas, R.B. (2018) Disentangling the effects of acidic air pollution, atmospheric CO_2, and climate change on recent growth of red spruce trees in the Central Appalachian Mountains. *Global Change Biology*, 24, 3938–3953.

Medvigy, D., Wofsy, S.C., Munger, J.W., Hollinger, D.Y. & Moorcroft, P.R. (2009) Mechanistic scaling of ecosystem function and dynamics in space and time: ecosystem Demography model version 2. *Journal of Geophysical Research*, 114, G01002.

Meinshausen, M., Smith, S.J., Calvin, K., Daniel, J.S., Kainuma, M.L.T., Lamarque, J.-F. et al. (2011) The RCP greenhouse gas concentrations and their extensions from 1765 to 2300. *Climatic Change*, 109, 213–241.

Muggeo, V.M. (2008). segmented: an R Package to Fit Regression Models with Broken-Line Relationships.

Nie, M., Lu, M., Bell, J., Raut, S. & Pendall, E. (2013) Altered root traits due to elevated CO_2: a meta-analysis. *Global Ecology and Biogeography*, 22, 1095–1105.

Norby, R.J., DeLucia, E.H., Gielen, B., Calfapietra, C., Giardina, C.P., King, J.S. et al. (2005) Forest response to elevated CO_2 is conserved across a broad range of productivity. *Proceedings of the National Academy of Sciences*, 102, 18052–18056.

Novick, K.A., Ficklin, D.L., Stoy, P.C., Williams, C.A., Bohrer, G., Oishi, A. et al. (2016) The increasing importance of atmospheric demand for ecosystem water and carbon fluxes. *Nature Climate Change*, 6, 1023–1027.

Oleson, K.W., Lawrence, D.M., Gordon, B., Flanner, M.G., Kluzek, E., Peter, J. et al. (2013) Technical description of version 4.5 of the Community Land Model (CLM). *NCAR/TN-478+STR NCAR Tech*. Note, 266.

Pan, Y., Birdsey, R.A., Fang, J., Houghton, R., Kauppi, P.E., Kurz, W.A. et al. (2011) A large and persistent carbon sink in the World's forests. *Science*, 333(6045), 988–993. https://doi.org/10.1126/science.1201609

Piao, S., Luyssaert, S., Ciais, P., Janssens, I.A., Chen, A., Cao, C. et al. (2010) Forest annual carbon cost: a global-scale analysis of autotrophic respiration. *Ecology*, 91, 652–661.

R Core Team (2018) R: a language and environment for Statistical Computing.

Reich, P.B., Sendall, K.M., Stefanski, A., Wei, X., Rich, R.L. & Montgomery, R.A. (2016) Boreal and temperate trees show strong acclimation of respiration to warming. *Nature*, 531, 633–636.

Reich, P.B., Tjoelker, M.G., Pregitzer, K.S., Wright, I.J., Oleksyn, J. & Machado, J.L. (2008) Scaling of respiration to nitrogen in leaves, stems and roots of higher land plants. *Ecology Letters*, 11, 793–801.

Rodell, M., Houser, P.R., Jambor, U., Gottschalck, J., Mitchell, K., Meng, C.-J. et al. (2004) The global land data assimilation system. *Bulletin of the American Meteorological Society*, 85, 381–394.

Schenk, H.J. & Jackson, R.B. (2002) The global biogeography of roots. *Ecological Monographs*, 72, 311–328.

Simard, M., Pinto, N., Fisher, J.B. & Baccini, A. (2011) Mapping forest canopy height globally with spaceborne lidar. *Journal of Geophysical Research*, 116, 1–12.

Slot, M., Rey-Sánchez, C., Gerber, S., Lichstein, J.W., Winter, K. & Kitajima, K. (2014) Thermal acclimation of leaf respiration of tropical trees and lianas: Response to experimental canopy warming, and consequences for tropical forest carbon balance. *Global Change Biology*, 20, 2915–2926.

Smith, N.G., Malyshev, S.L., Shevliakova, E., Kattge, J. & Dukes, J.S. (2016) Foliar temperature acclimation reduces simulated carbon sensitivity to climate. *Nature Climate Change*, 6, 407–411.

Stockfors, J. & Linder, S. (1998) Effect of nitrogen on the seasonal course of growth and maintenance respiration in stems of Norway spruce trees. *Tree Physiology*, 18, 155–166.

Swann, A.L.S., Hoffman, F.M., Koven, C.D. & Randerson, J.T. (2016) Plant responses to increasing CO_2 reduce estimates of climate impacts on drought severity. *Proceedings of the National Academy of Sciences*, 113, 10019–10024.

Taylor, K.E., Stouffer, R.J. & Meehl, G.A. (2012) An overview of CMIP5 and the experiment design. *Bulletin of the American Meteorological Society*, 93, 485–498.

Thorn, A.M., Xiao, J. & Ollinger, S.V. (2015) Generalization and evaluation of the process-based forest ecosystem model PnET-CN for other biomes. *Ecosphere*, 6, 1–27.

Trugman, A.T., Anderegg, L.D.L., Sperry, J.S., Wang, Y., Venturas, M. & Anderegg, W.R.L. (2019) Leveraging plant hydraulics to yield predictive and dynamic plant leaf allocation in vegetation models with climate change. *Global Change Biology*, 25, 4008–4021.

Trugman, A.T., Detto, M., Bartlett, M.K., Medvigy, D., Anderegg, W.R.L., Schwalm, C. et al. (2018) Tree carbon allocation explains forest drought-kill and recovery patterns. *Ecology Letters*, 21, 1552–1560.

Trugman, A.T., Medvigy, D., Anderegg, W.R.L. & Pacala, S.W. (2018) Differential declines in Alaskan boreal forest vitality related to climate and competition. *Global Change Biology*, 24, 1097–1107.

Venables, W.N. & Ripley, B.D. (2002) *Modern applied statistics with S*. Springer, New York: Fourth.

Walker, A.P., De Kauwe, M.G., Medlyn, B.E., Zaehle, S., Iversen, C.M., Asao, S. et al. (2019) Decadal biomass increment in early secondary succession woody ecosystems is increased by CO_2 enrichment. *Nature Communications*, 10, 454.

Walker, X. & Johnstone, J.F. (2014) Widespread negative correlations between black spruce growth and temperature across topographic moisture gradients in the boreal forest. *Environmental Research Letters*, 9(6), 064016. https://doi.org/10.1088/1748-9326/9/6/064016

Walker, X.J., Mack, M.C. & Johnstone, J.F. (2015) Stable carbon isotope analysis reveals widespread drought stress in boreal black spruce forests. *Global Change Biology*, 21, 3102–3113.

Wang, Y.P., Baldocchi, D., Leuning, R., Falge, E. & Vesala, T. (2007) Estimating parameters in a land-surface model by applying non-linear inversion to eddy covariance flux measurements from eight FLUXNET sites. *Global Change Biology*, 13, 652–670.

Way, D.A., Holly, C., Bruhn, D., Ball, M.C. & Atkin, O.K. (2015) Diurnal and seasonal variation in light and dark respiration in field-grown Eucalyptus pauciflora. *Tree Physiology*, 35, 840–849.

White, E.E., Ury, E.A., Bernhardt, E.S. & Yang, X. (2021) Climate change driving widespread loss of coastal forested wetlands throughout the north American coastal plain. *Ecosystems*, 1–16.

Yuan, W., Zheng, Y., Piao, S., Ciais, P., Lombardozzi, D., Wang, Y. et al. (2019) Increased atmospheric vapor pressure deficit reduces global vegetation growth. *Science Advances*, 5, eaax1396.

Zhang, Y., Xu, M., Chen, H. & Adams, J. (2009) Global pattern of NPP to GPP ratio derived from MODIS data: effects of ecosystem type, geographical location and climate. *Global Ecology and Biogeography*, 18, 280–290.

Zhu, Z., Piao, S., Myneni, R.B., Huang, M., Zeng, Z., Canadell, J.G. et al. (2016) Greening of the earth and its drivers. *Nature Climate Change*, 6(8), 1–6.

SUPPORTING INFORMATION

Additional supporting information may be found in the online version of the article at the publisher's website.